Technique to separate lidar signal and sunlight

Wenbo Sun,[1,*] Yongxiang Hu,[2] David G. MacDonnell,[2] Carl Weimer,[3] and Rosemary R. Baize[2]

[1]*Science Systems and Applications, Inc., Hampton, VA 23666, USA*
[2]*NASA Langley Research Center, Hampton, VA 23681, USA*
[3]*Ball Aerospace and Technologies Corp., Boulder, CO 80301, USA*
[*]*wenbo.sun-1@nasa.gov*

Abstract: Sunlight contamination dominates the backscatter noise in space-based lidar measurements during daytime. The background scattered sunlight is highly variable and dependent upon the surface and atmospheric albedo. The scattered sunlight contribution to noise increases over land and snow surfaces where surface albedos are high and thus overwhelm lidar backscatter from optically thin atmospheric constituents like aerosols and thin clouds. In this work, we developed a novel lidar remote sensing concept that potentially can eliminate sunlight induced noise. The new lidar concept requires: (1) a transmitted laser light that carries orbital angular momentum (OAM); and (2) a photon sieve (PS) diffractive filter that separates scattered sunlight from laser light backscattered from the atmosphere, ocean and solid surfaces. The method is based on numerical modeling of the focusing of Laguerre-Gaussian (LG) laser beam and plane-wave light by a PS. The model results show that after passing through a PS, laser light that carries the OAM is focused on a ring (called "focal ring" here) on the focal plane of the PS filter, very little energy arrives at the center of the focal plane. However, scattered sunlight, as a plane wave without the OAM, focuses at the center of the focal plane and thus can be effectively blocked or ducted out. We also find that the radius of the "focal ring" increases with the increase of azimuthal mode (L) of LG laser light, thus increasing L can more effectively separate the lidar signal away from the sunlight noise.

OCIS codes: (140.0140) Lasers and laser optics; (280.0280) Remote sensing and sensors; (230.0230) Optical devices; (050.0050) Diffraction and gratings.

References and links

1. D. L. Wu, J. H. Chae, A. Lambert, and F. F. Zhang, "Characteristics of CALIOP attenuated backscatter noise: implication for cloud/aerosol detection," Atmos. Chem. Phys. **11**(6), 2641–2654 (2011).
2. W. Sun, B. Lin, Y. Hu, C. Lukashin, S. Kato, and Z. Liu, "On the consistency of CERES longwave flux and AIRS temperature and humidity profiles," J. Geophys. Res. **116**(D17), D17101 (2011).
3. D. M. Winker, W. H. Hunt, and M. J. McGill, "Initial performance assessment of CALIOP," Geophys. Res. Lett. **34**(19), L19803 (2007).
4. W. Sun, G. Videen, S. Kato, B. Lin, C. Lukashin, and Y. Hu, "A study of subvisual clouds and their radiation effect with a synergy of CERES, MODIS, CALIPSO and AIRS data," J. Geophys. Res. **116**(D22), D2207 (2011).
5. W. Sun, G. Videen, and M. I. Mishchenko, "Detecting super-thin clouds with polarized sunlight," Geophys. Res. Lett. **41**(2), 688–693 (2014).
6. W. Sun, R. R. Baize, G. Videen, Y. Hu, and Q. Fu, "A method to retrieve super-thin cloud optical depth over ocean background with polarized sunlight," Atmos. Chem. Phys. **15**(20), 11909–11918 (2015).
7. H. H. Aumann, M. T. Chahine, C. Gautier, M. D. Goldberg, E. Kalnay, L. M. McMillin, H. Revercomb, P. W. Rosenkranz, W. L. Smith, D. H. Staelin, L. L. Strow, and J. Susskind, "AIRS/AMSU/HSB on the Aqua mission: Design, science objectives, data products, and processing systems," IEEE Trans. Geosci. Rem. Sens. **41**(2), 253–264 (2003).
8. L. Allen, M. W. Beijersbergen, R. J. C. Spreeuw, and J. P. Woerdman, "Orbital angular momentum of light and the transformation of Laguerre-Gaussian laser modes," Phys. Rev. A **45**(11), 8185–8189 (1992).
9. M. W. Beijersbergen, R. P. C. Coerwinkel, M. Kristensen, and J. P. Woerdman, "Helical-wavefront laser beams produced with a spiral phase plate," Opt. Commun. **112**(5–6), 321–327 (1994).
10. V. Y. Bazhenov, M. V. Vasnetsov, and M. S. Soskin, "Laser beams with screw dislocations in their wavefronts," JETP Lett. **52**(8), 429–431 (1990).

#262827 Received 8 Apr 2016; revised 19 May 2016; accepted 19 May 2016; published 3 Jun 2016

11. V. Y. Bazhenov, M. S. Soskin, and M. V. Vasnetsov, "Screw dislocations in light wavefronts," J. Mod. Opt. **39**(5), 985–990 (1992).
12. N. R. Heckenberg, R. McDuff, C. P. Smith, H. Rubinsztein-Dunlop, and M. J. Wegener, "Laser beams with phase singularities," Opt. Quantum Electron. **24**(9), S951–S962 (1992).
13. M. S. Soskin, V. Gorshkov, M. V. Vasnetsov, J. Malos, and N. Heckenberg, "Topological charge and angular momentum of light beams carrying optical vortices," Phys. Rev. A **56**(5), 4064–4075 (1997).
14. L. Marrucci, C. Manzo, and D. Paparo, "Optical spin-to-orbital angular momentum conversion in inhomogeneous anisotropic media," Phys. Rev. Lett. **96**(16), 163905 (2006).
15. E. Karimi, B. Piccirillo, E. Nagali, L. Marrucci, and E. Santamato, "Efficient generation and sorting of orbital angular momentum eigenmodes of light by thermally tuned q-plates," Appl. Phys. Lett. **94**(23), 231124 (2009).
16. L. Kipp, M. Skibowski, R. L. Johnson, R. Berndt, R. Adelung, S. Harm, and R. Seemann, "Sharper images by focusing soft X-rays with photon sieves," Nature **414**(6860), 184–188 (2001).
17. G. Andersen, "Large optical photon sieve," Opt. Lett. **30**(22), 2976–2978 (2005).
18. Y. Tang, S. Hu, Y. Yang, and Y. He, "Focusing property of high numerical aperture photon sieves based on vector diffraction," Opt. Commun. **295**, 1–4 (2013).
19. W. Sun, Y. Hu, C. Weimer, K. Ayers, R. R. Baize, and T. Lee, "A FDTD solution of scattering of laser beam with orbital angular momentum by dielectric particles: Far-field characteristics," J. Quant. Spectrosc. Radiat. Transf. in press.

1. Introduction

Ground-based, airborne and space-borne lidars are more and more applied in remote sensing applications and ranging practices. However, lidar measurements can be adversely affected by sunlight contamination during the daytime [1]. When lidar detectors receive scattered sunlight, they can be easily saturated, since solar radiation has enormous power on broad range of wavelengths. The sunlight-induced noise can be of orders higher than weak lidar return signals from bright surfaces such as landmass, snow and thick clouds. For optically thin atmospheric constituents like aerosols and super-thin clouds, sunlight contamination also can introduce large uncertainty in lidar measurements. As reported in Sun et al. [2]: Since NASA's Cloud-Aerosol Lidar and Infrared Pathfinder Satellite Observation (CALIPSO) lidar [3] cannot accurately detect super-thin clouds [2, 4–6] in daytime due to sunlight noise, the clear-sky and super-thin-cloudy-sky conditions cannot be well identified. This ambiguity in classifying sky conditions results in less accurate annual mean sea surface temperatures derived from NASA's Atmospheric Infrared Sounder (AIRS) [7] data for clear sky and for super-thin-cloudy sky, which incorrectly show that the annual mean sea surface temperatures for clear sky and for super-thin-cloudy sky to be very similar during the daytime. Because super-thin clouds should have significant effect on the AIRS-measured surface temperature [2], the close agreement observed between AIRS-measured surface temperature for clear-sky and super-thin-cloudy cases is most likely attributed to the error in the CALIPSO data. Without a robust technique to discriminate weak lidar signal from strong sunlight contamination, the quantitative data from daytime lidar measurements for optically thin compositions of the atmosphere have large uncertainties, though these are little reported. In this work, we developed a novel technique to spatially separate lidar signals from scattered background sunlight.

2. Method

Current lidar systems generally use a Gaussian beam (i.e. TEM_{00} mode) as wave source. The backscattered laser light is ultimately focused on the detector of a lidar system to become measurement signal. During daytime, the detector receives both the laser return signal and background sunlight. These photons, though from different sources, are focused on the same location on the sensor of a lidar, because a Gaussian beam return and the reflected plane-wave sunlight have little difference when they are received and focused by the receiving optical system of the lidar. Therefore, to separate lidar signal from sunlight contamination, we must fundamentally change the properties of the laser beam, so as to make the laser's reflection, refraction, diffraction, or focusing characteristics significantly different from sunlight. Based on this expectation, we did modeling of the focusing of sunlight, regular Gaussian lasers, and lasers with orbital angular momentum (OAM) [8–15] by a photon sieve (PS) [16, 17].

#262827 Received 8 Apr 2016; revised 19 May 2016; accepted 19 May 2016; published 3 Jun 2016

It's well known that a laser is an electromagnetic (EM) wave which can be made to carry orbital angular momentum (OAM) around the propagation direction [8–15], which can be approximated by the Laguerre-Gaussian (LG) beam as [8]

$$E(r,\varphi,z)=\frac{C_{Lp}}{w(z)}(\frac{r\sqrt{2}}{w(z)})^{|L|}\exp(-\frac{r^2}{w^2(z)})L_p^{|L|}(\frac{2r^2}{w^2(z)})$$
$$\times\exp(ik\frac{r^2}{2R(z)})\exp(iL\varphi)\exp[i(2p+|L|+1)\zeta(z)], \quad (1)$$

where C_{Lp} is a normalization constant; when the beam is normalized to unit power flux, $C_{Lp}=\sqrt{\frac{2p!}{\pi(p+|L|)!}}$, where the radial index $p\geq 0$ and the azimuthal index is L; $L_p^{|L|}$ are the generalized Laguerre polynomials; ϕ is the azimuth angle around the central axis of the beam; r is the radial distance from the central axis of the beam; z is the axial distance from the beam's narrowest point (the "waist"); *w(z)* is the radius at which the field amplitude drops to $1/e$ of their axial values, which has a form $w(z)=w_0\sqrt{1+(z/z_R)^2}$, where $z_R=\pi w_0^2/\lambda$, λ is the wavelength, and $w_0=w(0)$ is the waist size of the beam; *R(z)* is the radius of curvature of the beam's wave fronts, which has a form $R(z)=z[1+(z_R/z)^2]$; and $\zeta(z)$ is the Gouy phase shift, which defines a phase shift differing from that for a plane wave and has a form $\zeta(z)=\arctan(z/z_R)$. In this study, we use the purely azimuthal (the radial mode number p is assumed to be zero) Laguerre-Gaussian (LG) beams for the modeling. When L = 0, this is a regular Gaussian beam with maximum amplitude at the central axis. When $L \neq 0$, there is phase delay as function of ϕ around the central axis of the beam, which results in a spiral wave front of the EM beam and thus the beam has the OAM.

In this study, results are presented from the numerical simulation of the electric field of sunlight, a regular Gaussian beam, and a LG beams with OAM passing through a photon sieve (Fig. 1), conducted using the method for sum of pinhole-array-diffracted light reported in Tang et al [18].

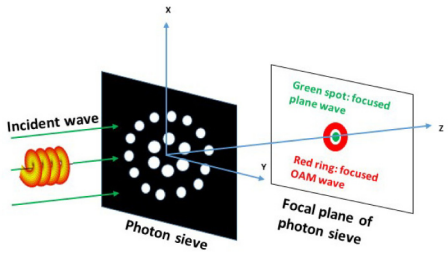

Fig. 1. Illustration of a photon sieve and light of plane wave and light with the OAM focused on the focal plane.

$$E_x(x,y,z)=\sum_{n=1}^{M}E_x^n(x,y,z), \quad (2a)$$

$$E_y(x,y,z)=\sum_{n=1}^{M}E_y^n(x,y,z), \quad (2b)$$

$$E_z(x,y,z)=\sum_{n=1}^{M}E_z^n(x,y,z), \quad (2c)$$

#262827 Received 8 Apr 2016; revised 19 May 2016; accepted 19 May 2016; published 3 Jun 2016

where $E_x^n(x,y,z)$, $E_y^n(x,y,z)$, and $E_z^n(x,y,z)$ are the diffracted electric field components from the n-th pinhole, given as

$$E_x^n(x,y,z) = r_n E_x(x_n,y_n) \times \int_0^k \exp(ikmz) J_0(r' k_r) J_1(r_n k_r) dk_r, \tag{3a}$$

$$E_y^n(x,y,z) = r_n E_y(x_n,y_n) \times \int_0^k \exp(ikmz) J_0(r' k_r) J_1(r_n k_r) dk_r, \tag{3b}$$

$$E_z^n(x,y,z) = -ir_n[E_x(x_n,y_n)\cos\alpha + E_y(x_n,y_n)\sin\alpha] \times \int_0^k \frac{k_r}{km} \exp(ikmz) J_0(r' k_r) J_1(r_n k_r) dk_r, \tag{3c}$$

where $E_x(x_n,y_n)$ and $E_y(x_n,y_n)$ are the incident field components at the n-th pinhole. r_n is the radius of the n-th pinhole which has a central position of (x_n,y_n) on the sieve. $i=\sqrt{-1}$ and $k=2\pi/\lambda$, where λ is the incident wavelength. $x-x_n = r'\cos\alpha$, $y-y_n = r'\sin\alpha$, where r' is the magnitude, and α is the azimuth angle (counted from x direction) of vector $(x-x_n, y-y_n, 0)$. $m=\sqrt{1-k_r^2/k^2}$ and k_r represents the wavenumber component (on the PS plane) of the diffracted light. $J_0(r'k_r)$ and $J_1(r_n k_r)$ are the 0th order and 1st order of Bessel function of first-kind, respectively. The radial position of the pinholes in the *n*-th ring is given as $R_n = \sqrt{2nf\lambda + (n\lambda)^2}$, where f is the focal plane distance from the photon sieve. $r_n = 1.53 f\lambda/(4R_n)$ in this simulation. The number of pinholes in the *n*-th ring is given as $N_{hole}^n = 0.5\{\alpha + \exp[-1/2(\beta 2n/N_{ring})^2]\}\pi R_1 r_1 / r_n^2$, where α = 0.8, β = 5.0, and N_{ring} is the total number of rings in the photon sieve.

3. Numerical results

Electric field intensity on the focal plane of a 75-ring pinhole sieve with a focal length of 5 mm at a wavelength of 1064 nm are shown in the left panel of Fig. 2, for a plane-wave (sunlight) incidence. We can see that, after passing through the PS, the plane wave remains well focused on the focal point. When the incidence is a regular Gaussian beam as described by Eq. (1) with p = 0, L = 0, and $w_0 = 300$ wavelength, we can see in the right panel of Fig. 2 that the laser is also focused within an area with a radius of ~5 μm from the focal point. Note here that for the plane-wave case, we assume the incident intensity per unit area is one unit, whereas for the LG beam incidence, we normalized the whole power of the beam to unit value. Comparing the two results in Fig. 2, we can see that a regular Gaussian beam cannot be spatially separated from the sunlight if the two lights come in the lidar receiver at the same time. This is similar to what happens at the focal point of the CALIPSO lidar focusing optical system.

#262827 Received 8 Apr 2016; revised 19 May 2016; accepted 19 May 2016; published 3 Jun 2016

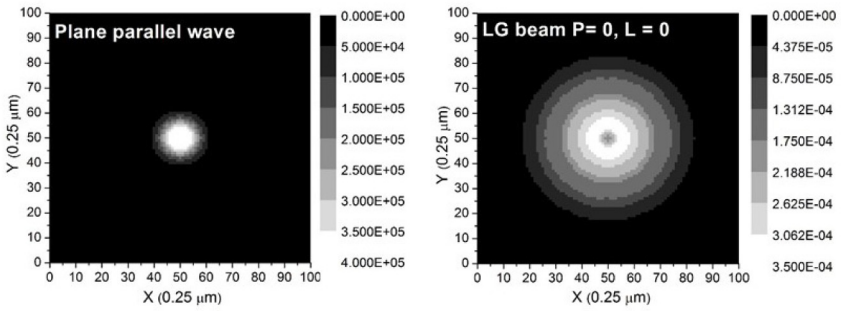

Fig. 2. Left panel: Intensity of electric field of a plane-wave light on the focal plane of a photon sieve; and right panel: Intensity of electric field of a regular Gaussian beam on the focal plane of a photon sieve.

However, if the laser has the OAM, i.e. $L \neq 0$ in Eq. (1), Fig. 3 shows that with the increase of L value, light intensity is distributed well off the focal point of the photon sieve. This is because the azimuthal phase difference of the OAM laser makes the pinhole-diffracted fields cancel each other in the constructive interference zone of the photon sieve, whereas constructively add in the destructive interference zone of the photon sieve, opposite to the photon sieve's behavior with sunlight or regular Gaussian laser light. When the LG laser has an $L = 7$, the laser is focused on a ring of ~10 μm off the focal point. Thus, using a photon sieve to filter incoming light and reading the data only on the outer ring can avoid most of the sunlight contamination to the lidar signal.

Although it is straightforward to know that the backscattered light can be distributed within a ring at the image plane if the scattering signal is from a ring laser's interaction with objects (aerosols), there is still reasonable concern with the conservation of laser's OAM state after its interaction with aerosol or cloud particles. From Eq. (1), we can see that the major factor that distinguishes the OAM laser from a regular Gaussian beam is $\exp(iL\varphi)$, which means that the OAM of light is mainly due to the azimuthal phase variation around the beam axis. No matter what kind of interaction the laser has with objects in its path, if the systematic phase difference for light around the beam axis is kept, the scattered light will still keep the OAM state. In lidar remote sensing, the backscattered light from different aersols which have equal optical distance from the laser source keeps the phase difference around its central axis at any time. Even when aerosols are not evenly distributed in the laser field, this can only alter the light intensity around the backscattered beam axis, but it cannot change the systematic phase difference. Therefore, we may not be able to see perfect laser ring backscattered from aerosols, but the laser speckles still keep the OAM and will not be focused on the focal point of the photon sieve.

#262827 Received 8 Apr 2016; revised 19 May 2016; accepted 19 May 2016; published 3 Jun 2016

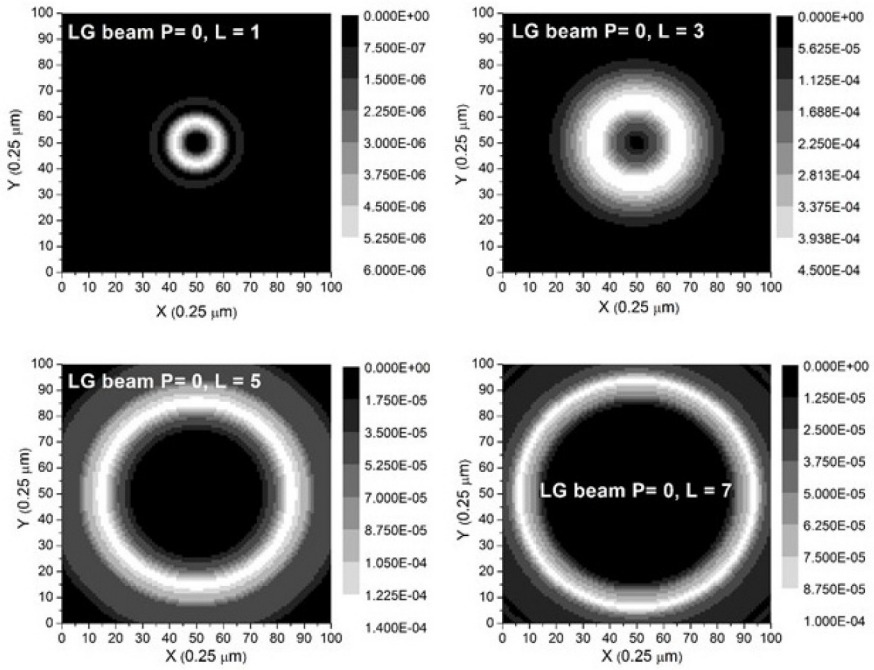

Fig. 3. Laser with orbital angular momentum (OAM) focused on the focal plane of a photon sieve. The LG laser is of L = 1, L = 3, L = 5, and L = 7, respectively. The spatial distribution of the light intensity is well off the focal point of the photon sieve when L > 5.

4. Conclusion

In summary, if incident light is natural light or polarized light (including linearly and circularly polarized light scattered from the Earth-atmosphere system), the light transferred through the photon sieve focuses on the focal point. However, if the light is a laser with orbital angular momentum (OAM), it does not focus on the focal point of the photon sieve, it focuses on a ring off the focal point. Using a laser with the OAM for the space-borne lidar, with the photon sieve filter, we can separate backscattered laser light and background sunlight noise. The interaction of the OAM laser with particles in the atmosphere was studied in Sun et al. [19], which shows some benefits of the OAM laser to be used in atmospheric remote sensing. Based on the concept reported here, a new generation of lidar system can be developed, which could significantly improve the daytime remote sensing of optically thin atmospheric compositions such as super-thin clouds, aerosols, water vapor, and CO2, etc. Note here that, the modeling results reported here are simply for demonstration of concept and for illustration of principle. The parameters for laser and photon sieve in this modeling are not based on actual instrumentation and may not be optimized ones for practice. An experiment to demonstrate the viability of this concept is being conducted in NASA Langley Research Center. The lab results will be documented in a subsequent report.

Acknowledgment

This work was supported by the Lab Demo (Photon Sieve) project of NASA Langley Research Center's IRAD and the OAM project of NASA ESTO ACT.

#262827 Received 8 Apr 2016; revised 19 May 2016; accepted 19 May 2016; published 3 Jun 2016